

Magneto- and barocaloric properties of the ferro-antiferromagnetic sawtooth chain

Nico Reichert,¹ Henrik Schlüter,¹ Tjark Heitmann,² Johannes Richter,^{3,4} Roman Rausch,⁵ and Jürgen Schnack^{1,*}

¹*Fakultät für Physik, Universität Bielefeld, Postfach 100131, D-33501 Bielefeld, Germany*

²*Fachbereich Mathematik/Informatik/Physik, Universität Osnabrück, Barbarastr. 7, D-49076 Osnabrück, Germany*

³*Institut für Physik, Otto-von-Guericke-Universität Magdeburg, P.O. Box 4120, D-39016 Magdeburg, Germany*

⁴*Max-Planck-Institut für Physik komplexer Systeme,
Nöthnitzer Straße 38, D-01187 Dresden, Germany*

⁵*Technische Universität Braunschweig, Institut für Mathematische Physik,
Mendelssohnstraße 3, D-38106 Braunschweig, Germany*

Materials that are susceptible to pressure and external magnetic fields allow the combined use of both for caloric processes. Here we report investigations of the ferromagnetic-antiferromagnetic sawtooth chain that due to its critical behavior not only allows for both barocaloric as well as magnetocaloric processes but also features very large cooling rates in the vicinity of the quantum critical point.

I. INTRODUCTION

Several archetypical frustrated spin systems such as the Heisenberg antiferromagnets on the kagome, square-kagome, pyrochlore or sawtooth lattice feature a flat energy band in one-magnon space [1–3], localized one-magnon energy eigenstates, and corresponding multi-magnon energy eigenstates [4]. These properties result in a macroscopic magnetization jump to saturation [5] as well as an increased magnetocaloric effect at the saturation field [6], non-ergodic dynamics [7], and other frustration effects [8]. For an overview see, e.g., Ref. [9].

The saturation field, however, is often not small and thus experimentally hard to reach. Fortunately, it turns out that for mixed ferromagnetic-antiferromagnetic interaction patterns models can be set up that feature similar properties at zero field [10, 11]. For the paradigmatic sawtooth (or equivalently delta) chain chemical compounds could be synthesized that resemble these properties rather closely [12, 13]. Meanwhile, the class of spin models featuring flat bands has been enlarged by moving to special XXZ [14, 15] or Dzyaloshinskii-Moriya couplings [16].

The critical properties of the ferromagnetic-antiferromagnetic sawtooth chain with ferromagnetic interaction $J_1 < 0$ between nearest neighbor spins as well as antiferromagnetic interaction $J_2 > 0$ between next nearest neighbor spins on even sites, compare Fig. 1, can be tuned via the coupling ratio $\alpha = J_2/|J_1| > 0$. For $0 \leq \alpha < \alpha_c = s_a/(2s_b)$ the ground state is given by the multiplet of the ferromagnetic state, i.e., with maximal total spin, whereas for $\alpha = \alpha_c$ the system features a quantum critical point (QCP) with macroscopic ground state degeneracy [10, 17, 18]. For $\alpha > \alpha_c$ the character of the ground state depends on whether the length of the sawtooth chain (with periodic boundary conditions) is a multiple of four or a multiple of two but not of four, compare [19, 20].

Since the density of states varies massively in the vicinity of the QCP the system exhibits a huge caloric effect. This will be discussed in III A. Experimentally, the ratio α can realistically be modified by means of pressure, that’s why we would like to term caloric effects due to a variation of α as barocaloric throughout this article. This dependence was already discussed in connection with the molecular ring molecule $\text{Fe}_{10}\text{Gd}_{10}$ [13] and is also observed for the antiferromagnetic sawtooth chain, see e.g. [21].

Here we want to extend the caloric phase diagram by additionally considering variations of the external magnetic field. To this end we investigate thermal equilibrium observables $\mathcal{O}(t, h, \alpha)$ as function of reduced temperature $t = T/|J_1|$, reduced magnetic field $h = g\mu_B B/|J_1|$, as well as “pressure” α . We will demonstrate that the combined use of barocaloric as well as magnetocaloric processes can lead to very large cooling rates in the vicinity of the QCP.

The paper is organized as follows. In Section II we introduce the model and major observables before we present our results in Sec. III. The article closes with a discussion in Section IV.

II. METHODS

A. The model

The sawtooth-chain Heisenberg model with periodic boundary conditions is given by the Hamiltonian

$$\begin{aligned} \tilde{H}' = & J_1 \sum_{i=0}^{N-1} \tilde{\mathbf{s}}_i \cdot \tilde{\mathbf{s}}_{i+1} + J_2 \sum_{i=0}^{N/2-1} \tilde{\mathbf{s}}_{2i} \cdot \tilde{\mathbf{s}}_{2i+2} \\ & + g\mu_B B \sum_{i=0}^{N-1} \tilde{s}_i^z, \end{aligned} \quad (1)$$

where $\tilde{\mathbf{s}}_i$ denotes the spin vector operator at site i , and a tilde is used to denote operators in general. We will consider the case where the exchange coupling $J_1 < 0$

* jschnack@uni-bielefeld.de

is ferromagnetic and the exchange coupling $J_2 > 0$ is antiferromagnetic, compare also Fig. 1.

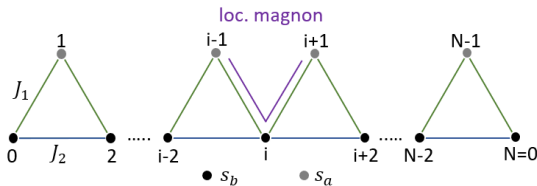


Figure 1. Structure of the sawtooth chain with apical spins s_a and basal spins s_b as well as ferromagnetic interaction J_1 and antiferromagnetic interaction J_2 . The spins are labeled $0, 1, \dots, N-1$. An independent localized one-magnon state, that is an eigenstate of the Hamiltonian, is depicted.

The coupling ratio $\alpha = J_2/|J_1| > 0$ allows to rewrite the Hamiltonian as

$$H = - \sum_{i=1}^N \vec{s}_i \cdot \vec{s}_{i+1} + \alpha \sum_{i=0}^{N/2-1} \vec{s}_{2i} \cdot \vec{s}_{2i+2} \quad (2)$$

$$+ h \sum_{i=0}^{N-1} \vec{s}_i^z,$$

with the dimensionless magnetic field $h = g\mu_B B/|J_1|$.

In the following we consider $s_a = s_b = s = 1/2$. Depending on the size N the system is treated with various methods. For $N \leq 24$ symmetries allow to obtain all energy eigenvalues and eigenvectors by means of exact numerical diagonalization of the Hamiltonian [22]. For $24 < N \lesssim 36$ the finite-temperature Lanczos method (FTLM) allows to determine low-lying energy eigenvalues as well as thermodynamic observables with high accuracy [23, 24]. For even larger sawtooth chains with $N > 36$ a flavor of the density matrix renormalization group theory (DMRG, [25, 26]) which employs $SU(2)$ symmetry is used to obtain ground state energies in subspaces of total spin S [20]. Thermodynamic properties are not investigated for such large systems.

B. Observables

The observables defined in the following section will be viewed as functions of the dimensionless model parameters α (related to pressure) and h (external field).

Low-temperature caloric figures of merit such as adiabatic temperature change, isothermal entropy change as well as the cooling rate are massively influenced by the structure of the low-energy density of states and as a special case of that by the degeneracy of the ground state [27, 28]. Since the model (1) is $SU(2)$ -invariant the total spin of the ground state gives rise to a $(2S+1)$ -degenerate multiplet at $h=0$ which is Zeeman-split by the magnetic field h . For instance, this led to a large ground state degeneracy of $(2S+1) = 121$ for $\text{Fe}_{10}\text{Gd}_{10}$ since its ground state spin is $S = 60$ [13]. A ground state

degeneracy immediately leads to a residual entropy at zero temperature, termed S_0 in the following. Isentropes of smaller entropy run into such points in the α - h -plane with decreasing temperature.

Besides the more trivial ground state degeneracy due to the multiplet structure of the energy spectrum a massive degeneracy of levels can be observed at the QCP. If such a degeneracy is exponential in N , the resulting residual entropy is extensive, i.e. scales with the size of the system N . This is relevant for macroscopic systems and the thermodynamic limit.

Since entropy $\mathcal{S}(t, h, \alpha)$ is a function of temperature, field and pressure,

$$\mathcal{S}(t, h, \alpha) = -k_B \text{Tr} \left[\tilde{\rho} \log(\tilde{\rho}) \right], \quad (3)$$

with $\tilde{\rho} = \tilde{\rho}(t, h, \alpha)$ being the density operator, two adiabatic cooling rates can be defined

$$\left(\frac{\partial t}{\partial h} \right)_{\mathcal{S}, \alpha} \quad \text{and} \quad \left(\frac{\partial t}{\partial \alpha} \right)_{\mathcal{S}, h}, \quad (4)$$

where the first expression quantifies the change of the temperature t with field and the second expression quantifies the change of the temperature t with pressure on a two-dimensional isentrope surface (\mathcal{S} isosurface).

III. RESULTS

A. Ground state properties and quantum critical point

For $0 \leq \alpha = J_2/|J_1| < \alpha_c = s_a/(2s_b)$ the ground state is given by the multiplet of the fully polarized, i.e. ferromagnetic state. For N spins of spin quantum number $s = 1/2$ this would yield a ground state spin of $S_0 = N/2$. For $\alpha > \alpha_c$ the character of the ground state depends on whether the lengths of the sawtooth chain (with periodic boundary conditions) is a multiple of four or a multiple of two but not of four, at least for $s = 1/2$, compare [19, 20]. Figure 2 displays this behavior for a selection of smaller systems (always with periodic boundary conditions). The result of the top panel was already discussed in Ref. [20]: The ground state spin drops to zero for large α in case of sawtooth chains where the length is a multiple of four. Cases of even length where the length is not divisible by four behave differently. Here the ground state spin assumes a non-zero value for large α ; for N spins $s = 1/2$ this would be $(N+2)/4$. The underlying reason is that the basal spins form a spin ring of odd length whose approximate ground state spin is $1/2$ for large α [29]. The apical spins are then polarized accordingly due to the ferromagnetic interaction.

For $\alpha = \alpha_c$ the system features a quantum critical point (QCP) with macroscopic ground state degeneracy [10, 18] and a very dense low-lying spectrum. Figure 3 displays this behavior for the case of 24 spins

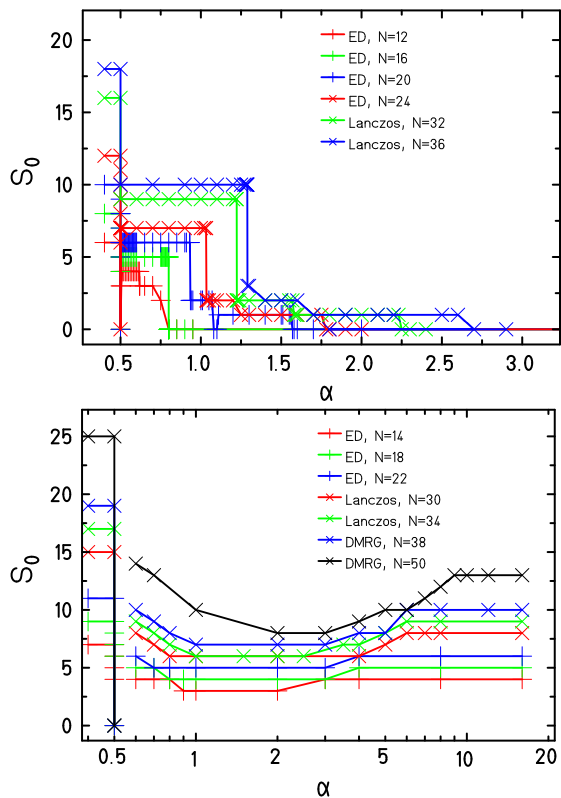


Figure 2. Ground-state spin quantum number S_0 for various α and selected lengths N that are multiples of four (top) or multiples of two, but not of four (bottom). Depending on the length exact diagonalization (ED), Lanczos diagonalization (Lanczos), or $SU(2)$ density-matrix renormalization group theory (DMRG) was employed. The lines are drawn as a guide for the eye.

$s = 1/2$. The lowest 50 eigenvalues are shown for selected values of α except for $\alpha = 1/2$, where the lowest 10,000 eigenvalues are displayed. The collapse of the spectrum for $\alpha \rightarrow \alpha_c$ is the reason for the remarkable caloric properties of the system in the vicinity of this quantum critical point. The degenerate ground state contains the multiplets of many spin quantum numbers, $S_0 \in \{0, S_{0,\min}, \dots, S_{0,\max}\}$, where e.g. for (all even) N spins $s = 1/2$ $S_{0,\max} = N/2$ and for N being a multiple of four $S_{0,\min} = N/4 + 1$.

B. Magneto- and barocaloric phase diagram

While the quantum phase transition at $\alpha = \alpha_c, h = 0$ yields a macroscopic ground state degeneracy, further points of ground state degeneracy can be found in the α - h -plane. For each α , an external magnetic field h splits all multiplets according to the respective magnetic quantum number M . If $M = -N/2$ (for N spins with $s = 1/2$) is not already the energetically lowest state for $\alpha > 0.5$, compare example in Fig. 3, crossings appear whenever magnetic levels of higher-lying multiplets

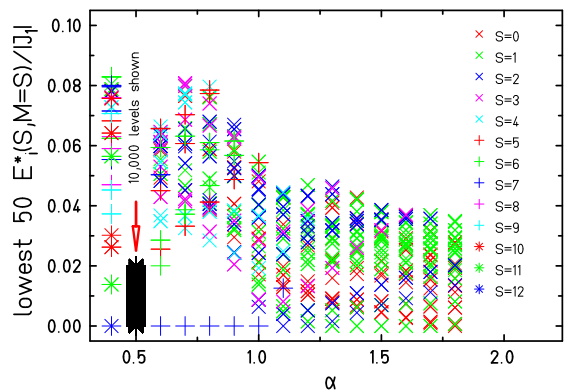


Figure 3. Example of low-lying energy levels for $N = 24$ as function of α : Only the lowest 50 eigenvalues are shown for selected values of α except for $\alpha = 1/2$, where the lowest 10,000 eigenvalues are displayed. The intention is to picture the very untypical density of states at the QCP for $\alpha = 1/2$.

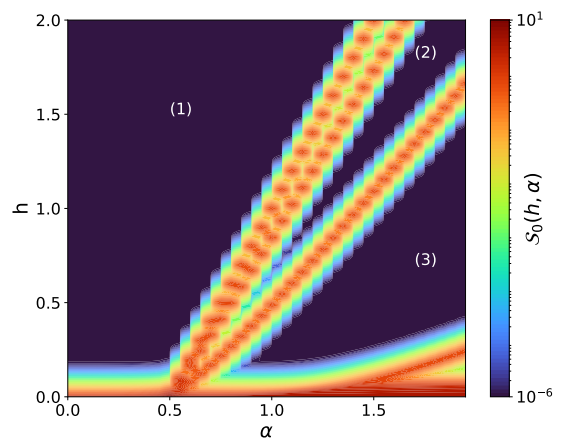


Figure 4. Map of (near) ground state entropy for $N = 16$ and $s = 1/2$ as function of α and h (logarithmic scale). The entropy was evaluated at $t = 0.01$ for technical reasons. At $\alpha = 0.5, h = 0$ the quantum critical point is visible. The dotted curves that move towards the upper right corner separate areas with ground state spins $S_0 \in \{S_{0,\max}, \dots, S_{0,\min}\}$ from left to right; here in particular $S_0 = 8$ in (1), $S_0 = 6$ in (2), and $S_0 = 5$ in (3), compare also Fig. 5. The light region for larger $\alpha > 1$ and almost vanishing field h reflects a growing low-lying density of states consisting of excitations with $S \in \{0, \dots, 4\}$.

become new ground states. For those multiplets that are part of the degenerate ground state at the QCP, this yields curves of level crossings in the α - h -plane that head towards the QCP, compare Fig. 4 and Fig. 5 as well as discussion below.

The whole scenario can be pictured by means of an entropy map as displayed in Fig. 4 for the case of $N = 16$ and $s = 1/2$. The near ground state entropy is color-coded on a logarithmic scale; it was evaluated at $t = 0.01$ for technical reasons. At $\alpha = 0.5, h = 0$ the quantum critical point is visible. The reddish curves separate ar-

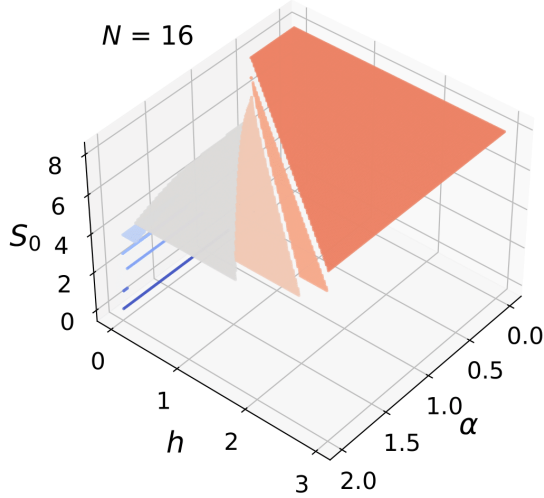


Figure 5. Ground state spin S_0 for $N = 16$ and $s = 1/2$ as function of α and h .

states with ground state spins $S_0 \in \{S_{0,\max}, \dots, S_{0,\min}\}$ from left to right. For larger $\alpha > 1$ and almost vanishing field h the reddish curves reflect a with α growing low-lying density of states consisting of excitations with smaller total spin, here $S \in \{0, \dots, 4\}$. In addition, the spectrum splits into bunches of levels with further increasing α since the system progressively turns into an antiferromagnetic ring and loosely attached, almost free apical spins, compare also [30]. This is reflected by the upturning branch at low fields and $\alpha > 1.25$.

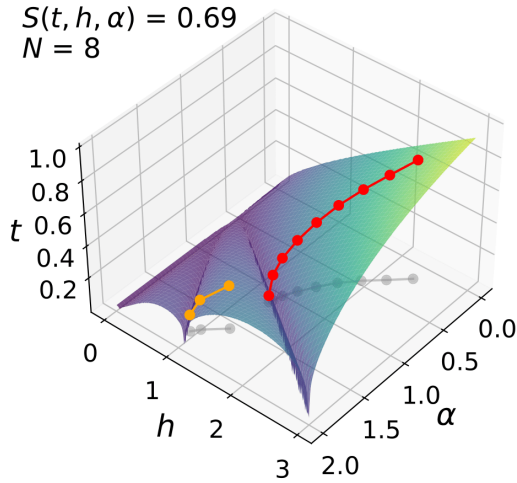


Figure 6. Isentrope surface with $S(t, h, \alpha) = 0.69 < \log(2) \approx 0.693$ in the parameter-space of α , h , and t . The dotted curves represent processes of steepest descent on which cooling rates assume maximal values.

The change of ground state spin quantum numbers can also be assessed by looking at Fig. 5, where S_0 is dis-

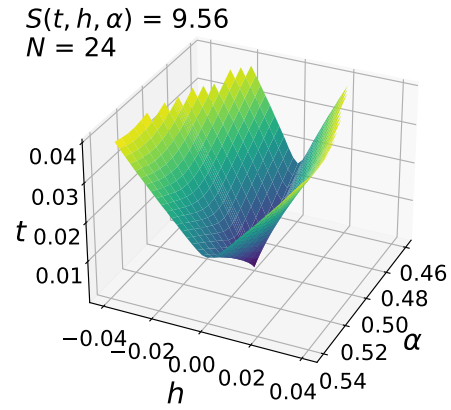
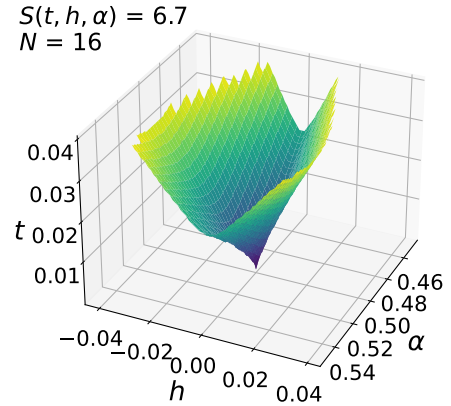
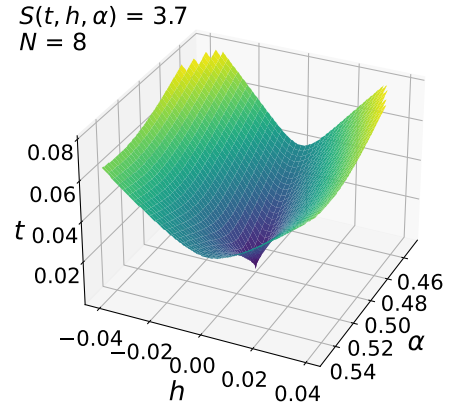


Figure 7. Isentrope surfaces in the parameter-space of α , h , and t in the vicinity of the QCP for $N = 8$ (top), $N = 16$ (middle), and $N = 24$ (bottom) and entropy values close to the residual entropy at the QCP. $N = 8$: $S = 3.7 < \log(41) \approx 3.714$, $N = 16$: $S = 6.7 < \log(817) \approx 6.706$, $N = 24$: $S = 9.56 < \log(14260) \approx 9.565$.

played in terms of colored planes as function of α and h . The above discussed ground state degeneracies happen at the steps between planes of constant S_0 of which the rightmost three run towards the QCP at $\alpha = 0.5$, $h = 0$ since the respective multiplets are part of the degenerate ground state.

Moving from zero to non-zero temperatures the sys-

tems allows many interesting thermodynamic processes in particular since the iso-entropy (isentropic) surfaces are strongly curved and feature cusps for low temperatures, compare Fig. 6 for a small system with $N = 8$ and $s = 1/2$. In contrast to purely barocaloric or purely magnetocaloric systems, a magnetic quantum critical system offers processes with very large cooling rates when pressure and field are modified simultaneously in order to achieve a steepest descent on an isotrope surface. Two such processes are depicted in Fig. 6 by curves of connected bullet points.

A close-up look at the vicinity of the quantum critical point in Fig. 7 shows that isentropes close to the value corresponding to the degeneracy of the QCP assume very large slopes towards zero temperature. These isentrope surfaces mark the quantum critical region inside which one observes universal behavior, i.e. no scale is provided by system parameters, only temperature controls the behavior, and the fluctuations possess classical character, see also [31, Fig. 1 (r.h.s.)] or [32, Fig. 1 (l.h.s.)]. For $\alpha \neq 0.5$, a system-specific low-energy scale emerges due to frustration that can be orders of magnitude smaller than the involved parameters of the system such as $J_{1/2}$ [33, 34]. Here for $\alpha > 0.5$, quantum fluctuations dominate whereas for $\alpha < 0.5$ a ferromagnetic ordering exists at zero temperature only [31]. As one can see in Fig. 7 and in accordance with [31] the quantum critical region gets narrower with increasing system size. This is related to the fact that the residual entropy for $\alpha \neq 0.5$ scales roughly like $\log(N)$ whereas for $\alpha = 0.5$ at the QCP it scales approximately like N . This suggests that the largest cooling rates are only achievable in very close proximity to the QCP.

IV. DISCUSSION

Materials that are susceptible to pressure and external magnetic fields allow the combined use of both for caloric

processes, compare Refs. [35–37] for related recent examples. This might, e.g., be advantageous when running single-shot cooling experiments or thermodynamic cycles with field and pressure sweeps. Spin systems such as the discussed ferromagnetic-antiferromagnetic sawtooth chain offer the additional feature of a quantum critical point, whereby in the vicinity of this point cooling rates are particularly large. In the space of external parameters α (related to pressure) and h (magnetic field) this special point can be approached from various directions, not only via change of pressure which provides more experimental options.

Quite recently, the idea to employ magneto-electric couplings was formulated for the sawtooth chain in order to drive the ratio of the two exchange interactions towards the critical value [16]. This would enable one to use the material more closely to the QCP and thus to benefit from much larger cooling rates. Altogether, the electric field could replace pressure to drive α . One could then speak of a magneto-electric drive where one can apply both magnetic as well as electric fields to steer the thermodynamic processes.

ACKNOWLEDGMENT

This work was supported by the Deutsche Forschungsgemeinschaft DFG (355031190 (FOR 2692); 397300368 (SCHN 615/25-2); RI 615/25-1 and 449703145 (SCHN 615/28-1)).

-
- [1] H. Tasaki, Ferromagnetism in the Hubbard models with degenerate single-electron ground states, *Phys. Rev. Lett.* **69**, 1608 (1992).
 - [2] A. Mielke, Exact ground-states for the Hubbard-model on the kagome lattice, *J. Phys. A-Math. Gen.* **25**, 4335 (1992).
 - [3] A. Mielke and H. Tasaki, Ferromagnetism in the Hubbard-model – examples from models with degenerate single-electron ground-states, *Commun. Math. Phys.* **158**, 341 (1993).
 - [4] J. Schnack, H.-J. Schmidt, J. Richter, and J. Schulenburg, Independent magnon states on magnetic polytopes, *Eur. Phys. J. B* **24**, 475 (2001).
 - [5] J. Schulenburg, A. Honecker, J. Schnack, J. Richter, and H.-J. Schmidt, Macroscopic magnetization jumps due to independent magnons in frustrated quantum spin lattices, *Phys. Rev. Lett.* **88**, 167207 (2002).
 - [6] M. E. Zhitomirsky and A. Honecker, Magnetocaloric effect in one-dimensional antiferromagnets, *J. Stat. Mech.: Theor. Exp.*, P07012 (2004).
 - [7] F. Johannesmann, J. Ecksele, H. Schlüter, and J. Schnack, Nonergodic one-magnon magnetization dynamics of the antiferromagnetic delta chain, *Phys. Rev. B* **108**, 064304 (2023).
 - [8] P. Mendels, D. Bono, F. Bert, O. Garlea, C. Darie, P. Bordet, V. Brouet, M.-H. Julien, A.-D. Hillier, and A. Amato, Oxygen doped $s = 1/2$ Cu delafossites: a muon spin rotation/relaxation study, *J. Phys.: Condens. Matter* **16**, S799 (2004).
 - [9] O. Derzhko, J. Richter, and M. Maksymenko, Strongly correlated flat-band systems: The route from Heisenberg spins to Hubbard electrons, *Int. J. Mod. Phys. B* **29**, 1530007 (2015).

- [10] V. Y. Krivnov, D. V. Dmitriev, S. Nishimoto, S.-L. Drechsler, and J. Richter, Delta chain with ferromagnetic and antiferromagnetic interactions at the critical point, *Phys. Rev. B* **90**, 014441 (2014).
- [11] D. V. Dmitriev and V. Y. Krivnov, Magnetic properties of delta- and kagome-like chains with competing interactions, *J. Phys.: Condens. Matter* **35**, 445802 (2023).
- [12] Y. Inagaki, Y. Narumi, K. Kindo, H. Kikuchi, T. Kamikawa, T. Kunimoto, S. Okubo, H. Ohta, T. Saito, M. Azuma, M. Takano, H. Nojiri, M. Kaburagi, and T. Tonegawa, Ferro-antiferromagnetic delta-chain system studied by high field magnetization measurements, *J. Phys. Soc. Jpn.* **74**, 2831 (2005).
- [13] A. Baniodeh, N. Magnani, Y. Lan, G. Buth, C. E. Anson, J. Richter, M. Affronte, J. Schnack, and A. K. Powell, High spin cycles: topping the spin record for a single molecule verging on quantum criticality, *npj Quantum Materials* **3**, 10 (2018).
- [14] H. J. Changlani, D. Kochkov, K. Kumar, B. K. Clark, and E. Fradkin, Macroscopically degenerate exactly solvable point in the spin-1/2 kagome quantum antiferromagnet, *Phys. Rev. Lett.* **120**, 117202 (2018).
- [15] H. J. Changlani, S. Pujari, C.-M. Chung, and B. K. Clark, Resonating quantum three-coloring wave functions for the kagome quantum antiferromagnet, *Phys. Rev. B* **99**, 104433 (2019).
- [16] J. Richter, V. Ohanyan, J. Schulenburg, and J. Schnack, Electric field driven flat bands: Enhanced magnetoelectric and electrocaloric effects in frustrated quantum magnets, *Phys. Rev. B* **105**, 054420 (2022).
- [17] D. V. Dmitriev and V. Y. Krivnov, Delta chain with anisotropic ferromagnetic and antiferromagnetic interactions, *Phys. Rev. B* **92**, 184422 (2015).
- [18] O. Derzhko, J. Schnack, D. V. Dmitriev, V. Y. Krivnov, and J. Richter, Flat-band physics in the spin-1/2 sawtooth chain, *Eur. Phys. J. B* **93**, 161 (2020).
- [19] T. Tonegawa and M. Kaburagi, Ground-state properties of an $s = 1/2$ δ -chain with ferro- and antiferromagnetic interactions, *J. Magn. Magn. Mater.* **272-276**, Part 2, 898 (2004).
- [20] R. Rausch, M. Peschke, C. Plorin, J. Schnack, and C. Karrasch, Quantum spin spiral ground state of the ferromagnetic sawtooth chain, *SciPost Phys.* **14**, 052 (2023).
- [21] T. Nakamura and S. Takada, Relaxation of frustration and gap enhancement by the lattice distortion in the Δ chain, *Phys. Lett. A* **225**, 315 (1997).
- [22] T. Heitmann and J. Schnack, Combined use of translational and spin-rotational invariance for spin systems, *Phys. Rev. B* **99**, 134405 (2019).
- [23] J. Jaklič and P. Prelovšek, Lanczos method for the calculation of finite-temperature quantities in correlated systems, *Phys. Rev. B* **49**, 5065 (1994).
- [24] J. Schnack, J. Richter, and R. Steinigeweg, Accuracy of the finite-temperature Lanczos method compared to simple typicality-based estimates, *Phys. Rev. Research* **2**, 013186 (2020).
- [25] S. R. White, Density matrix formulation for quantum renormalization groups, *Phys. Rev. Lett.* **69**, 2863 (1992).
- [26] U. Schollwöck, The density-matrix renormalization group in the age of matrix product states, *Annals of Physics* **326**, 96 (2011).
- [27] L. Zhu, M. Garst, A. Rosch, and Q. Si, Universally diverging Grüneisen parameter and the magnetocaloric effect close to quantum critical points, *Phys. Rev. Lett.* **91**, 066404 (2003).
- [28] J. W. Sharples, D. Collison, E. J. L. McInnes, J. Schnack, E. Palacios, and M. Evangelisti, Quantum signatures of a molecular nanomagnet in direct magnetocaloric measurements, *Nat. Commun.* **5**, 5321 (2014).
- [29] K. Bärwinkel, H.-J. Schmidt, and J. Schnack, Ground state properties of antiferromagnetic Heisenberg spin rings, *J. Magn. Magn. Mater.* **220**, 227 (2000).
- [30] V. Y. Krivnov and D. V. Dmitriev, Spin triangle chain with ferromagnetic and antiferromagnetic interactions on the transition line, *J. Phys.: Condens. Matter* **35**, 095802 (2022).
- [31] T. Vojta, Quantum phase transitions in electronic systems, *Ann. Phys.* **9**, 403 (2000).
- [32] M. Vojta, Quantum phase transitions, *Rep. Prog. Phys.* **66**, 2069 (2003).
- [33] X. Obradors, A. Labarta, A. Isalgué, J. Tejada, J. Rodriguez, and M. Pernet, Magnetic frustration and lattice dimensionality in $\text{SrCr}_8\text{Ga}_4\text{O}_{19}$, *Solid State Commun.* **65**, 189 (1988).
- [34] A. P. Ramirez, Strongly geometrically frustrated magnets, *Annu. Rev. Mater. Sci.* **24**, 453 (1994).
- [35] J. Guo, G. Sun, B. Zhao, L. Wang, W. Hong, V. A. Sidorov, N. Ma, Q. Wu, S. Li, Z. Y. Meng, A. W. Sandvik, and L. Sun, Quantum phases of $\text{SrCu}_2(\text{BO}_3)_2$ from high-pressure thermodynamics, *Phys. Rev. Lett.* **124**, 206602 (2020).
- [36] J. L. Jiménez, S. P. G. Crone, E. Fogh, M. E. Zayed, R. Lortz, E. Pomjakushina, K. Conder, A. M. Läuchli, L. Weber, S. Wessel, A. Honecker, B. Normand, C. Rüegg, P. Corboz, H. M. Rønnow, and F. Mila, A quantum magnetic analogue to the critical point of water, *Nature* **592**, 370 (2021).
- [37] J. Wang, H. Li, N. Xi, Y. Gao, Q.-B. Yan, W. Li, and G. Su, Plaquette singlet transition, magnetic barocaloric effect, and spin supersolidity in the Shastry-Sutherland model, *Phys. Rev. Lett.* **131**, 116702 (2023).